Development of the CTF3 photo-injector laser system

G. Kurdi, I. O. Musgrave, M. Divall, E. Springate, W. Martin, G. J. Hirst and I. N. Ross
Central Laser Facility, STFC, Rutherford Appleton Laboratory, Chilton, Didcot, Oxfordshire, OX11 0QX, UK

Main contact email address I.O.Musgrave@rl.ac.uk

Introduction

The CTF3 photo-injector laser system is designed to deliver high power, microsecond long trains of ultraviolet laser pulses to the photo-cathode of the CTF3 accelerator. The initial section of the accelerator will operate at 1.5 GHz, before using a ring combiner to double this to 3 GHz. A further combiner ring is then used to multiply this to 30 GHz. This places a number of particular requirements on the laser. It has to be synchronized to an external RF source and be capable of generating pulses that are temporally structured. The temporal structure of the pulses is of a 1.5 μs macropulse envelope containing ~2300 of the 1.5 GHz repetition rate micropulses. The macropulse will be divided into bunches of pulses that are 141ns long and phase coded. The phase coding essentially temporally shifts each bunch of pulses by half a pulse repetition time (333ps) with respect to the previous bunch so that when the electron bunches are interleaved in the first combiner ring they produce a 3 GHz signal, this cannot be achieved with conventional cathodes. The temporal complexity of the output requires the system to be very stable. The system will run at up to 50 Hz macropulse repetition rate, delivering 15 kW pulse train mean power in the IR. This light will then be converted into the UV (262nm). The system requirements are shown in Table 1.

Target Parameters	Units	CTF3
Oscillator repetition rate	GHz	1.5
Macropulse width	μs	1.548
Macropulse repetition rate	Hz	5/50
Energy at cathode per pulse	nJ	370
IR/UV conversion efficiency	%	7.4
IR energy per pulse	μJ	10
IR pulse train mean power	kW	15
IR average power (at 50 Hz)	W	200
UV average power (at 50 Hz)	mW	86

Table 1. System requirements for CTF3 Photo-injector laser.

System description

The layout of the whole laser system is shown in figure 1. A Nd:YLF passively mode-locked oscillator and CW preamplifier system has been purchased [1], producing 6 ps pulses at a 1.5 GHz repetition rate at 1047 nm with an average power of 320 mW after the oscillator and 10 W after the preamplifier. The oscillator and pre-amplifier can be synchronised to an external reference source with a time jitter <1ps. A high speed fibre modulator will be placed between the laser oscillator and preamplifier system to allow phase coding of the 1.5 GHz pulse train. Preliminary measurements indicate that this will reduce the output to ~6 W.

The output of the oscillator and preamplifier system will then be amplified in a series of two Nd:YLF diode-pumped power amplifiers. In the first amplifier, we pump with 15 kW of diode power in 400 μs pulses to reach a pulse-train mean power of 3 kW (2 μJ per micropulse). The second amplifier, where we pump with 20 kW of diode power in 200 μs pulses, has a gain of five to give an output pulse-train mean power of 15 kW. The output pulse trains are then gated with a fast Pockels cell to produce 1.55 μs, flat-top pulse trains, before second and then fourth harmonic generation.

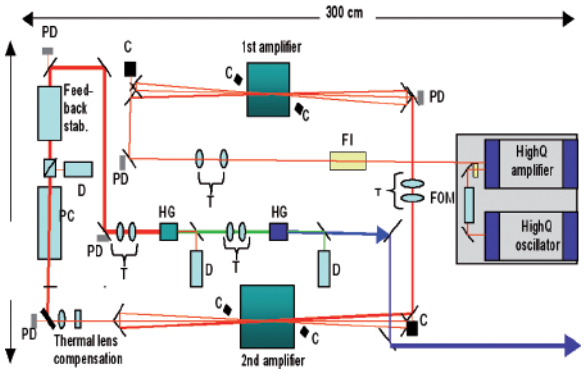

Figure 1. Layout of the laser system. FOM, fibre-optic modulator, FI, Faraday isolator; T, telescope; PD, calibrated photodiode for power monitoring; C, camera to monitor alignment; PC, Pockels cell to produce 1.55 μs flat-top pulse train; D, diagnostics; HG, harmonic generation crystal.

Amplifier design and performance

The amplifier head design is based upon the designs discussed in detail by Tang *et al.* [2]. A photograph of the first amplifier head is shown in figure 3 (left). The design consists of a Nd:YLF laser rod mounted in a glass tube that is filled with cooling water. Surrounding this tube are 5 diode stacks. The diode stacks are aligned so that the fast axis is aligned parallel to the length of the rod. A cylindrical lens is placed at the output of the diode stacks to bring the slow axis light to an approximate waist in the rod. The parameters of the two amplifier heads are listed in Table 2.

The fluorescence distribution in the rod for pumping with individual diode arrays and with all five diode arrays together is shown in figure 3 (centre) for the first amplifier. The light from the diodes at an angle to the crystal axes generates mixed polarizations. This has an impact because the absorption for light polarized parallel to the c-axis is a factor of two higher than that polarized perpendicular to it. The effect of the diode polarization is visible, with the diodes closest to the horizontal (Fig 3 (centre) c,d) being most strongly absorbed. When we pump with all five diodes, the five-fold geometry and slight offset of each diode from the centre-line of the rod

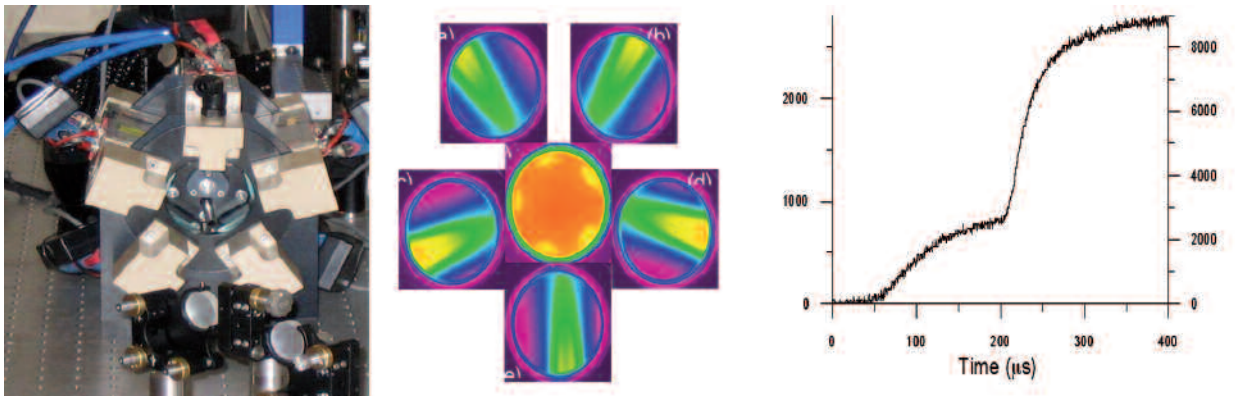

Figure 3. Left: Photograph of the first amplifier head. Centre Measured fluorescence distribution from each of the five diodes individually (a-e) and from all five diodes together (f). Right: Measured gain and mean power of the two amplifiers.

enable us to obtain a pumping uniformity of nearly 80% over the total area of the rod. Amplifier 2 demonstrates similar behaviour.

	1st amplifier	2nd amplifier
Diameter of the rod	7 mm	10 mm
Effective pump length	7 cm	11 cm
Total peak pumping power	18 kW	25 kW
Repetition rate	1-50 Hz	1-50 Hz
Max. duty cycle	2.5%	2%
Max. average pumping power	450 W	500 W
Number of passes	3	3
Gain	300	5

Table 2. Amplifier head parameters.

We have measured the gain of the first amplifier in single pass and compared the results against the predictions of the code previously developed to model diode pumped amplifiers[3]. The measurements show good agreement with the code, except at the highest input and pump powers when the measured gain is ~80% of that predicted. This discrepancy between the code and measurements suggests that the model for ASE used in the code is not correct. However, we still obtain sufficient gain. With the design values of 6800 mW input power and 15.8 kW pump power, we measure a single-pass gain of >200. The amplifier is designed to run with three passes of the rod (as shown in figure 1) and this multi-pass configuration has also been assembled and tested. We use a telescope to focus weakly into the rod, giving beam diameter of 1 mm in the rod at the first pass. The beam then expands through the amplifier to give beam sizes of 2 mm and 3 mm on the second and third passes respectively. At the full input power and diode pump power, the gain saturates at 525 after 300 ms giving an output power of 3390 W. This compares well with the design input power to the second amplifier of 3 kW. The performance of the second amplifier has not come quite so close to specification, we have so far achieved a gain of 4 and the output power appears to become clamped at 9 kW as shown in figure 3 (right). At the present moment we are not certain of the cause of this, one cause could be significant ASE in the amplifier.

To achieve the high temporal stability required the amplifier design is based on a saturated quasi steady-state operation. The model is discussed in detail in[3]. The measured multipass gain and mean power of the two amplifiers is shown in figure 3 (right). As can be seen after 400 µs the output of the two amplifiers is steady state. To achieve this, the diodes of the first amplifier are switched on 125 µs after those for the first amplifier.

We have also measured the beam profiles after the two amplifier stages as shown in Figure 4. As can be seen the beam diameter increases with increasing pump power due to saturation. The beam profile is affected by inhomogeneities we believe these are caused by the Nd:YLF rod in the first amplifier, however the profile is acceptably smooth.

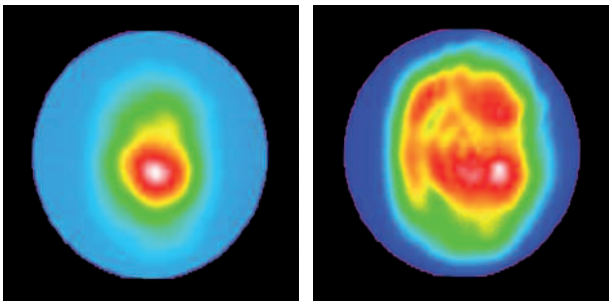

Figure 4. Comparison of un-amplified (left) and amplified (right) beam profiles.

One important advantage of Nd:YLF is its weak thermal lens compared to other solid state laser media, such as Nd:YAG[5]. The time between pulses is so short compared to the thermal time constant of either rod that essentially no temperature decay takes place between macropulses. The temperature profile is then identical to that obtained at CW operation for the same input power. Assuming uniform pumping along the length of the rod and around its circumference, this sets up a temperature profile which is highest in the centre of the rod and decreases quadratically with radius[6]. With 10 litres/min cooling water flow, we calculate a temperature difference between the centre and edges of the rod of 16°C at 50 Hz operation.

The two major contributions to the thermal lens are the change in refractive index and length of the rod with temperature. Stress-induced birefringence is not believed to be a major contributor to thermal lensing in Nd:YLF because of the large natural birefringence of the crystal[7].

The change in refractive index with temperature is negative and different along each of the two axes, so this contributes a negative, astigmatic lens. However, the bulging end faces of the rod give a positive lens which partially offsets this. Not all of the length of the rod is free to expand because it is constrained by the rest of the rod. For example a section in the middle of the rod will, try to expand but will also be under compressive forces from the sections of the rod either side of it. Therefore we assume that only the end-sections expand. The effective length of the expanding section of the rod varies from one laser to another depending on the way the rod is held and other material parameters. Our estimates give focal lengths of >10 m when the rod is pumped at 5 Hz. The thermal lens should increase linearly with thermal load, unless energy transfer upconversion is significant, in which case a stronger thermal lens increasing nonlinearly with pump power would be expected [7]. We have carried out initial measurements of thermal lensing in the first amplifier, using a Phasics SID4 wavefront sensor. These confirm that at 5 Hz operation , the focal length of the thermal lens is well over 10 m.

Optical gating

To produce a flat-top 1.55 µs pulse-train from the ~250 µs steady state portion of the macropulses we use a BBO Pockels cell. The accelerator requirements dictate rise and fall times of the macropulses to be just 2 – 3 ns. The Pockels cell must also be designed to handle the high average power and capable of producing a flat-top output pulse. We have chosen a BBO Pockels cell because it combines high power handling and low piezo-electric effect. However, the incident average power when the amplifiers run at the full 50 Hz repetition rate will be in excess of 2 $kWcm^{-2}$, which is high even for BBO. To reduce this load we use an acousto-optic modulator (AOM) to dump as much excess power as possible before the Pockels cell. Fused silica AOMs have high laser damage thresholds and very low thermal and photo-elastic induced birefringence, so should provide very stable transmission. The AOM will be switched on to dump the excess power in the macropulse before and after the selected 1.5 µs pulse–train period and off during the pulse, relaxing the requirements on stability of the RF. To reduce the half wave voltage the pockels cell will contain two crystals in series. The stability of the voltage produced by the Pockels cell driver is specified as 5% within 20 ns of switch-on and 1% during the flat-topped pulse. The ringing in the voltage at switch-on should be fixed pulse-to-pulse, so we are considering the option of using an arbitrary waveform generator and secondary Pockels cell to compensate for this as part of the stabilization scheme.

Phase Coding

In this section we describe the method by which we generate the phase coding. The output from the oscillator is coupled into polarizing maintaining fibre and injected into an intensity modulator as shown in figure 5. The modulator is based on a Mach-Zehnder interferometer and is used to generate pulses that have a duration of ~140ns. The output from the modulator is then divided into two using a 50/50 coupler. The two outputs are then injected into fibre delay lines which have different lengths. The first has a relatively short length, 2m, and forms the green sections of the phase-coded output. The second fibre is longer, 30m, and generates a delay of 140ns. This forms the red sections of the phase-coded signal. This phase coded signal is then injected into the pre-amplifier system.

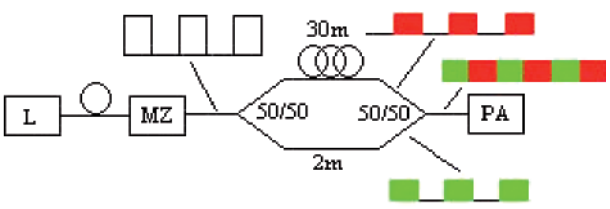

Figure 5. Schematic of the phase coding scheme. L: Laser, MZ: Mach-Zehnder intensity modulator, PA: Pre-amplifier.

To allow for drifts and the tolerances of manufacture the longer delay loop was mounted onto a resistively heated mount. By varying the temperature of the longer delay it is possible to change the delay between the two arms. Figure 6 shows some measurements of the characterization of the phase coding system undertaken so far. The upper trace of figure 6 shows the output of the coding system without the intensity modulator. With the mode-locked pulse train going through just the fibre delay lines you would expect a signal to be generated at 3 GHz. However a suitable RF spectrum analyzer was unavailable to confirm this. The trace shows the signal generated by a fibre-coupled photodiode. As can be seen the resolution of the system is limited to viewing the 6ps pulses of the oscillator as ~50ps pulses. In figure 6 (upper) the pulses from both halves of the coding scheme can be seen with the signal from one arm being attenuated by loosening the connection between two fibres these are the pulses that have gone through the shorter delay line. The blue trace was obtained with the long delay length at room temperature the magenta trace was achieved with the temperature of the long fibre increased to 40°C. Using this technique we were able to shift the pulses relative to each other by 50ps for a 15° temperature change. The lower trace of figure 6 shows a test to determine the relative delay between the two fibre lengths. This was achieved by using the modulator to generate pulses shorter than the relative delay, so the time between leading edges could be determined and thereby the relative delay. These measurements show that the relative delay is approximately 150ns, however at the time

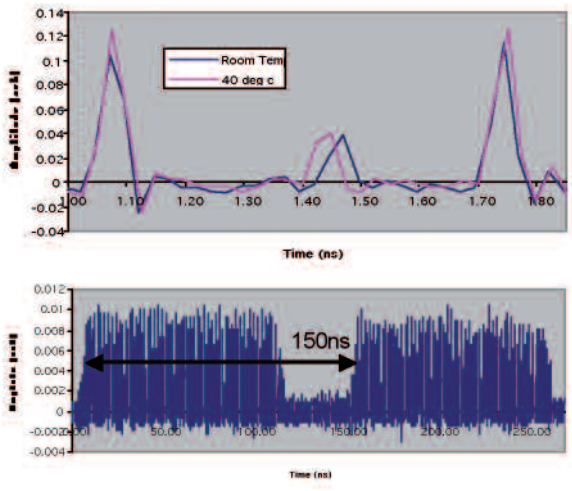

Figure 6. Upper Variation of relative delay between delay lines with temperature. Lower Measurement of absolute delay of large fibre length.

of the measurement the 2m was not in the system which would reduce this. The shape of the leading edge is due to the electrical signal used to operate the MZ modulator.

Conclusions

High power diode-pumped Nd:YLF amplifiers running in quasi steady state mode, based on a common concept of pump head geometry, have been designed and developed. We have measured output powers in excess of 9 kW after three passes of the two amplifier heads. The design is based on quasi-steady state operation because of the high stability required, and the measured output reaches the steady-state after ~300 ms. Calculations based on a simplified model show reasonable agreement with experimental results, giving us a good guideline for further development and optimization of laser performance. We have constructed a system for optical gating with sufficient temporal stability to generate the required 1.55μs macropulses. The fibre phasecoding system has undergone initial tests and shown to prove the principle of operation. We will undertake further tests to determine if either of the fibre lengths require modification. Our early experiments with the non-linear stages that have not been reported here have shown encouraging results and suggest that although we had lower than expected IR performance we will still be able to deliver the required UV pulses.

We acknowledge the support of the European Community-Research Infrastructure Activity under the FP6 "Structuring the European Research Area" programme (CARE, contract number RII3-CT-2003-506395).

References

1. M. Divall *et al*., CARE-Report-05026-PHIN.
2. Tang *et al*., CLF Annual Report 2004/2005.
3. I. N. Ross and M.Csatari, CLF Annual Report 2001/2002 202-205 (2002).
4. I. Will, A. Liero, D. Mertins, W. Sandner, *IEE J Quant Elec*, **34**, 2020 (1998).
5. J. E.Murray, *IEEE J Quant Elec*, **19**, 488 (1983).
6. W. Koechner, *"Solid-State Laser Engineering"*, Springer.
7. P. J. Hardman *et al*., *IEEE J Quant Elec,* **35**, 647 (1999).